APL Materials

Out-of-plane transport in ZrSiS and ZrSiSe microstructures

Cite as: APL Mater. **7**, 101116 (2019); https://doi.org/10.1063/1.5124568
Submitted: 15 August 2019 . Accepted: 19 September 2019 . Published Online: 17 October 2019

Kent R. Shirer, Kimberly A. Modic, Tino Zimmerling, Maja D. Bachmann, Markus König, Philip J. W. Moll, Leslie Schoop, and Andrew P. Mackenzie

APL Materials ARTICLE scitation.org/journal/apm

Out-of-plane transport in ZrSiS and ZrSiSe microstructures

Cite as: APL Mater. 7, 101116 (2019); doi: 10.1063/1.5124568
Submitted: 15 August 2019 • Accepted: 19 September 2019 •
Published Online: 17 October 2019

Kent R. Shirer,[1,a)] Kimberly A. Modic,[1] Tino Zimmerling,[1] Maja D. Bachmann,[1,2] Markus König,[1] Philip J. W. Moll,[1,3] Leslie Schoop,[4] and Andrew P. Mackenzie[1,2]

AFFILIATIONS

[1]Max Planck Institute for Chemical Physics of Solids, 01187 Dresden, Germany
[2]School of Physics and Astronomy, University of St. Andrews, St. Andrews KY16 9SS, United Kingdom
[3]Institute of Materials, École Polytechnique Fédérale de Lausanne (EPFL), 1015 Lausanne, Switzerland
[4]Princeton University, Princeton, New Jersey 08544, USA

Note: This paper is part of the Special Topic on Topological Semimetals—New Directions.
[a)]**Electronic mail:** kent.shirer@cpfs.mpg.de

ABSTRACT

A recent class of topological nodal-line semimetals with the general formula MSiX (M = Zr, Hf and X = S, Se, Te) has attracted much experimental and theoretical interest due to their properties, particularly their large magnetoresistances and high carrier mobilities. The plateletlike nature of the MSiX crystals and their extremely low residual resistivities make measurements of the resistivity along the [001] direction extremely challenging. To accomplish such measurements, microstructures of single crystals were prepared using focused ion beam techniques. Microstructures prepared in this manner have very well-defined geometries and maintain their high crystal quality, verified by the observations of quantum oscillations. We present magnetoresistance and quantum oscillation data for currents applied along both [001] and [100] in ZrSiS and ZrSiSe, which are consistent with the nontrivial topology of the Dirac line-node, as determined by a measured π Berry phase. Surprisingly, we find that, despite the three dimensional nature of both the Fermi surfaces of ZrSiS and ZrSiSe, both the resistivity anisotropy under applied magnetic fields and the in-plane angular dependent magnetoresistance differ considerably between the two compounds. Finally, we discuss the role microstructuring can play in the study of these materials and our ability to make these microstructures free-standing.

I. INTRODUCTION

Materials which exhibit nontrivial topology or linear dispersion relations in their band structures such as topological insulators, graphene, and Dirac and Weyl semimetals have attracted intense interest in the past 15 years for their exotic properties, potential technological applications, and possible topological superconductivity.[1–8] Recently, a class of topological materials which host Dirac band crossings along nodal lines or loops, distinct from the discrete Dirac points of Dirac and Weyl semimetals, have been predicted and discovered,[9–13] and resulting experimental[14–25] and theoretical[26–28] studies have demonstrated these materials to be excellent candidates for both application and the study of new, novel physics.

Of the nodal-line materials, those with the general formula MSiX (M = Zr, Hf and X = S, Se, Te), layered materials which have a PbFCl-type structure with space group *P*4/*nmm*, have attracted particular attention due to their large magnetoresistances, unusual transport behaviors, relatively cheap and easy synthesis, and other exotic properties.[10,17,20–22] The most studied of these, ZrSiS, has both a 3D nodal-line state and a nonsymmorphic symmetry-protected 2D Dirac node, where the nodal-lines are located near the Fermi level, and its linearly dispersing bands extend over a large energy range (0–2 eV).[10,14] The 2D Dirac state, in contrast, is located ~0.5 eV below the Fermi level. Therefore, the physics of the material is thought to be determined by the nodal-line states.[15,22] Furthermore, the ZrSiX-type materials provide a testing ground to explore the

relationship between dimensionality of the Fermi surface and the topological character of the materials.

In these materials, as X is varied from S to Te, the strength of the interlayer bond decreases by an order of magnitude and the accompanying *c*/*a*-ratios are 2.27, 2.30, and 2.59.[9,29] A crossover from 3D to 2D behavior is therefore thought to occur between Se and Te.[9] The Fermi surfaces of ZrSiS and ZrSiSe are three-dimensional although they seem to possess pockets which also have a 2D character.[10,20,21,25] The recent suggestion of correlated physics in ZrSiS and ZrSiSe[22,26–28] also provides motivation for in- and out-of-plane transport measurements, which have revealed surprising new states in correlated systems.[30–32] Given the thin, platelet-like nature of ZrSiS and ZrSiSe crystals, precision measurements that utilize FIB microstructures, devices made from single crystals with current paths well-defined by a focused ion beam, are desirable.[30,33]

Here, we present magnetoresistance and quantum oscillation data in ZrSiS and ZrSiSe for currents applied along [100] and [001] simultaneously in FIB microstructured devices up to 14 T for applied magnetic fields in a number of orientations in and out-of-plane. We find a significant difference in the behavior of both the angular dependent in-plane magnetoresistance and also the resistivity anisotropy between ZrSiS and ZrSiSe. We observe that for currents along [001], the magnetoresistance decreases above 2 T. We also show a nontrivial Berry phase from quantum oscillation measurements for currents applied in [100] and [001]. These measurements provide insight into the anisotropic transport properties of these materials, which may have implications for our fundamental understanding of topological line-node semimetals and possible device applications.

II. EXPERIMENTAL METHODS

Single crystals of ZrSiS and ZrSiSe were grown using chemical vapor transport. Stoichiometric amounts of Zr, Si, and S (or Se) were sealed in a carbon coated quartz tube, together with a small amount of iodine as a transport agent. The sealed tube was heated in a single zone tube furnace to 1100 C, where a temperature gradient of approximately 100 C was measured between the hot and the cold end of the tube. Crystals grew within 1 week at the hot end. The crystals were then washed with isopropanol and subsequently annealed at 600 C for three weeks. The composition and structure was confirmed with x-ray diffraction and EDX and was aligned using Laue diffraction. The sample quality is evident from their low residual resistivities and the observation of quantum oscillations. Aligned crystals were mounted so that a slab—a "lamella"—could be extracted and then structured into mesoscopic transport devices using a Ga^{2+} FEI Helios G3 CX focused ion beam instrument (FIB). This microstructuring procedure consists of a number of steps, as illustrated in Figs. 1(a)–1(h) with an SEM image of such a structure shown in Fig. 1(i). The steps are (a) lamella cutting, (b) undercutting and polishing, (c) *ex-situ* extraction, (d) transfer to the substrate, (e) gold deposition and platinum reinforcement, (f) gold removal, (g) oxygen plasma cleaning, and (h) final structuring. In the lamella cutting step, trenches are cut with a beam current of 9.3 nA and a voltage of 30 kV into the aligned single crystal, leaving an approximately 100 μm long, 50 μm wide, and 5 μm thick crystal lamella. Note that this lamella can be oriented along an arbitrary crystallographic direction appropriate for the measurement. The lamella is then undercut and polished at a lower current of 2.5 nA. It is later transferred *ex-situ* under an optical microscope with a Kapton needle onto a sapphire or Si/SiO_2 substrate with lithographically prepared gold leads. A thin epoxy droplet is used to fix the lamella to the substrate. The device is then sputter-coated with 200 nm of gold through a shadow mask which provides electrical contact between the lamella and gold leads.

In the case of ZrSiSe and ZrSiS materials, sub-ohm contact resistances are consistently achieved through this method. Bridges of platinum are then deposited with the FIB to reinforce the gold once the structure is free-standing. Without the platinum reinforcement,

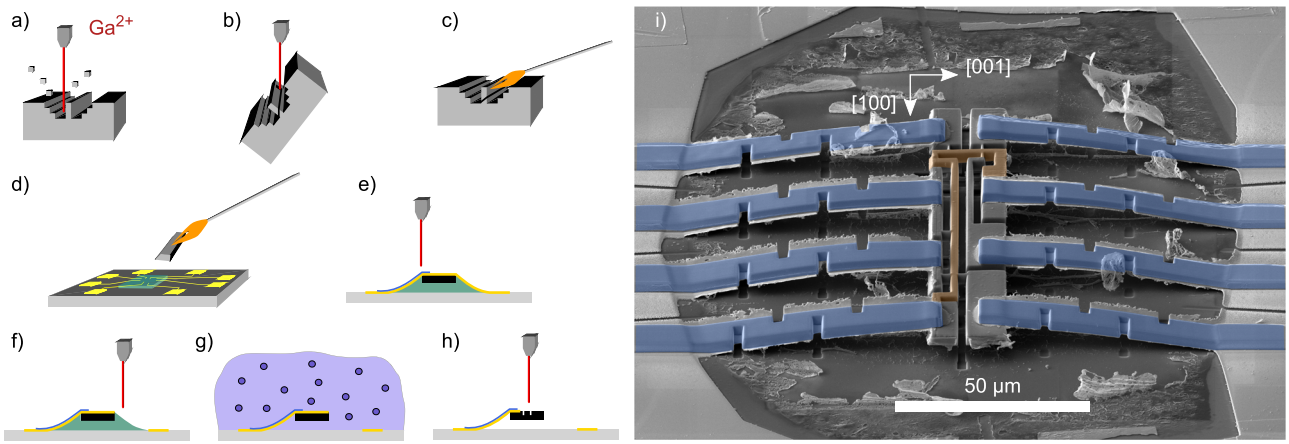

FIG. 1. Focused ion beam process for free-standing microstructures: [(a)–(h)] Cartoon of the process to extract a lamella from the bulk crystal and create a free standing microstructure as explained in the text. (i) The right panel shows a false-color SEM image of a microstructured device of single crystal ZrSiSe used in the experiment. The current path is highlighted in orange, the gold contacts are highlighted in light gray, and the platinum bridges are highlighted in blue. The crystal was carefully aligned such that four-point resistance bars are along the [100] and [001] directions, as illustrated.

the gold tends to tear. Excess gold is removed to expose as much epoxy area as possible, and then the device is exposed to an oxygen plasma treatment for 5–15 min, depending on the amount of epoxy to be removed. The device is then structured a final time in the FIB with cuts to define electrical transport bars along [100] or [001], using a current of 800 Pa. Both free-standing samples and samples coupled to the substrate with epoxy were tested and produced similar results.

Resistivity data were taken in four point measurement configurations for a number of samples for each compound. Magnetotransport measurements along specific crystalline directions in ZrSiS and ZrSiSe samples, highly conductive metals with $\rho_a|_{T=0K} \approx 200$ nΩ cm and $\rho_a|_{T=0K} \approx 1$ μΩ cm, respectively, are difficult and require a precise sample geometry. Our microstructured samples allow us to control the sample geometry on a sub-micrometer scale to provide a total device resistance of ~1 Ω. Combined with extremely low contact resistances, we thus achieve a very high signal-to-noise ratio, evident in Figs. 3–5 and in the raw data shown in the supplementary material. The samples were measured in a 14 T quantum design Physical Property Measurement System (PPMS) with a horizontal rotator using external lock-in amplifiers from Zurich Instruments. Currents of 100 μA and 500 μA with lock-in frequencies of 177.77 and 233.33 Hz were used for simultaneous measurements to check consistency of multiple samples. For clarity, we use the convention that magnetic fields applied along [100] or [001] are parallel to current applied along the same direction in the device, while a magnetic field applied along [010] is perpendicular to both directions.

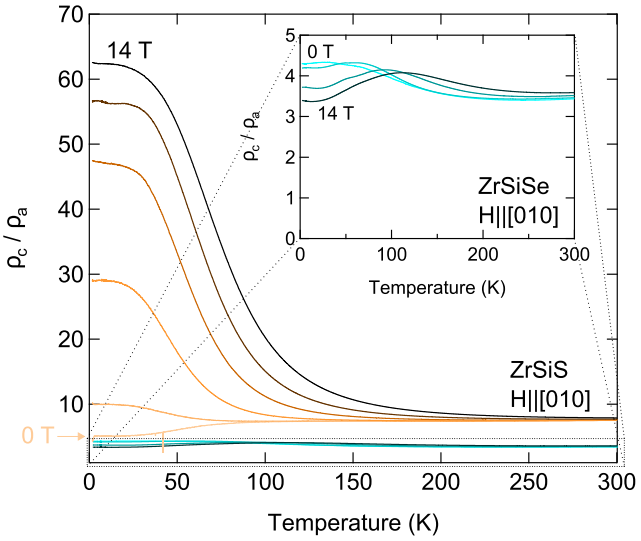

FIG. 2. Resistivity anisotropy for fields applied along [010]: The resistivity anisotropy in ZrSiS is shown with increasing applied magnetic fields of 0, 1, 3, 6, 10, and 14 T. In the absence of field, it is roughly constant from 2 to 300 K. In the presence of applied field along [010], the resistivity anisotropy increases substantially at low temperatures. In contrast, the resistivity anisotropy of ZrSiSe (teal lines) is insensitive to magnetic fields applied along [010]. The inset shows the detailed temperature dependence of the resistivity anisotropy of ZrSiSe at fields of 0, 4, 9, and 14 T.

III. RESULTS

Here, we report four main experimental observations. The first is the strong difference in resistivity anisotropy between ZrSiS and ZrSiSe under applied magnetic fields. In the absence of magnetic field, the resistivity anisotropy in both compounds is moderate, ~8 and ~4, for ZrSiS and ZrSiSe, respectively, and does not vary substantially with temperature. In the presence of applied magnetic field along [010], the difference between the two compounds in resistivity anisotropy is striking, shown in Fig. 2 and in the supplementary material. In this case, the resistivity anisotropy, ρ_c/ρ_a, of ZrSiS grows to more than 60, while that of ZrSiSe is virtually unchanged. When the field is applied along [001], both compounds exhibit similar resistivity anisotropies of ~0.1 (see top left insets of Figs. 4 and 5). When field is applied along [100], the resistivity anisotropy is again similar, ~100.

The sensitive dependence of the resistivity anisotropy on applied magnetic field in ZrSiS is closely related to our second experimental observation, the in-plane angular dependence of the magnetoresistance. Figure 3 shows the angular dependence of the magnetoresistance for fields applied perpendicular to [001], rotated from [010] to [100] for currents along [100] and [001]. When current is applied along [001], the responses of ZrSiS and ZrSiSe are virtually identical. Their resistivity shows a four-fold, cloverlike symmetry that reaches nearly 400 μΩ cm at 14 T when the field is applied along [100] and [010] with a small enhancement of the resistivity for fields along [110]. This small enhancement along [110] grows with increasing applied field. Additionally, oscillatory components of the resistivity are evident above 9 T, probably due to the sensitive angular dependent nature of quantum oscillations on the small, three dimensional pockets of the Fermi surface. For measurements with current applied along [100], however, the magnetoresistance of ZrSiS and ZrSiSe behaves in remarkably distinct fashions. In the case of ZrSiS, the in-plane magnetoresistance has a slightly asymmetric, cloverlike shape that varies only mildly from 4.5 μΩ cm for $H \parallel [010]$ to 3 μΩ cm for $H \parallel [100]$. In ZrSiSe, the magnetoresistance is twofold symmetric, with a dumbbell-like shape. For fields along [010], the resistivity grows to more than 100 μΩ cm, while along [100], the resistivity barely changes from its zero-applied field value. Previous measurements of resistivity for currents applied along [100] for applied fields rotated from [100] to [001] (a different orientation than reported here) in both ZrSiS and ZrSiSe have shown a "butterfly shaped" magnetoresistance pattern due to a convolution of two- and fourfold symmetries present in each compound.[15,17] In contrast, the differences between the angular dependence of the in-plane magnetoresistances may be due to an increased two-dimensionality (2D) when S is replaced with Se.[9,15,34] Further measurements investigating ZrSiTe could verify if this trend remains consistent in an even more two-dimensional structure.

Our third and fourth experimental observations are those of a nontrivial Berry curvature for both compounds with currents along [100] and [001] in applied fields along [001] and an abrupt decrease in the magnetoresistance of ZrSiS and ZrSiSe above 2 T for currents applied along [001] with a parallel applied field. While the Dirac-line node has been observed through angle-resolved photoemission spectroscopy (ARPES) and through measurements of a Berry phase from magnetization, resistivity, or thermoelectric

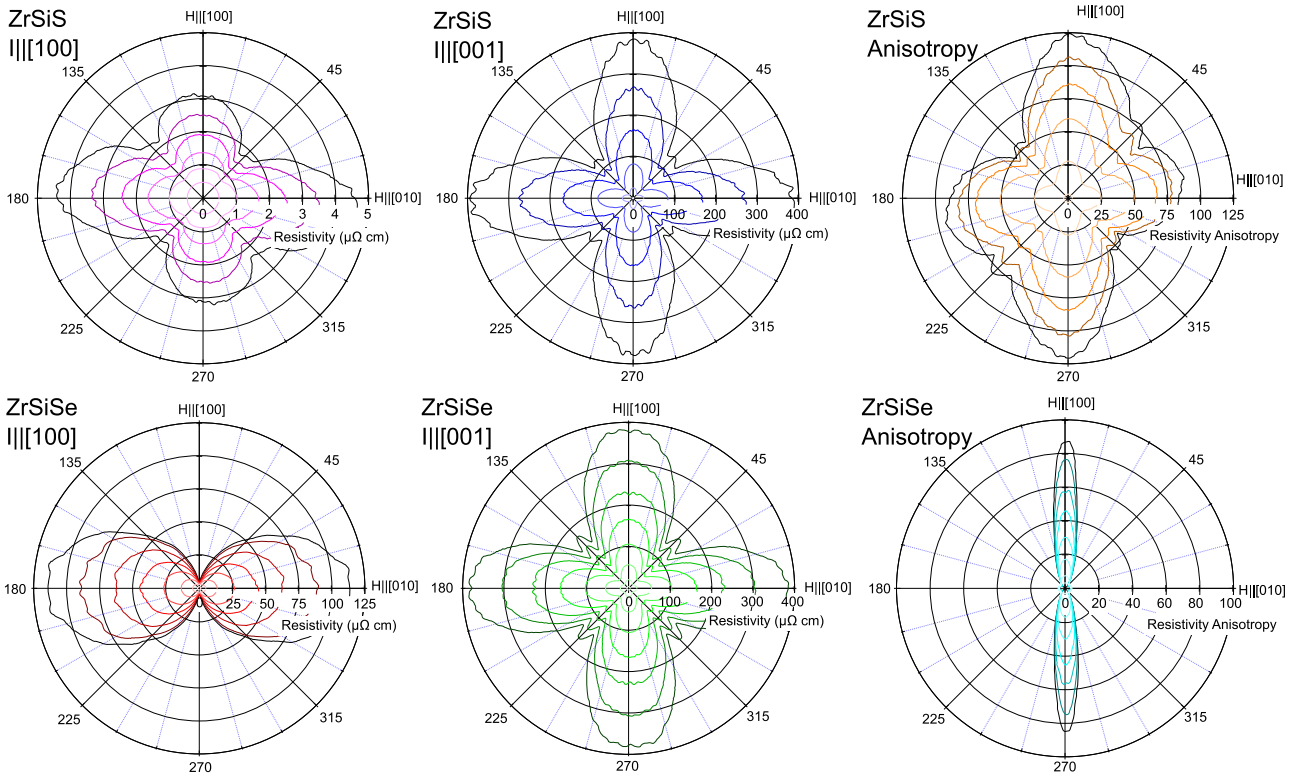

FIG. 3. Polar plots: Angular dependent magnetoresistance for in-plane magnetic fields [010] (0°) to [100] (90°) for currents applied along [100] and [001]. Curves are taken at 1.8 K for fields of 0, 2.8, 5.6, 8.4, 11.2, and 14 T, light to dark colors, for ZrSiS and for fields of 0, 2, 4, 6, 8, 10, 12, 14 T for ZrSiSe. Polar plots of the resistivity anisotropy are also shown.

measurements before,[10,14–17,19–23] we are not aware of any resistivity measurements for currents applied along [001] where Shubnikov–de Haas (SdH) oscillations, those oscillations of the resistivity which arise from the quantization of quasiparticle cyclotron orbits with increasing magnetic field, are observed. Furthermore, the high aspect-ratio of our device gives a sufficiently high signal-to-noise ratio to measure such oscillations with high precision. This allows us to verify that our focused ion beam manufactured devices remain of high single-crystal quality, which may have implications for future functional device applications.

The Shubnikov–de Haas oscillation amplitude can be described by[1,7]

$$\frac{\Delta\rho_{xx}}{\rho} \propto R_S R_T R_D \cos\left[2\pi\left(\frac{F}{B}+\frac{1}{2}+\beta\pm\delta_{LK}\right)\right], \quad (1)$$

where $R_S = \cos\left(\frac{\pi g^* m^*}{2m_e(1+\lambda_{e-ph})}\right)$, $R_T = \frac{(2\pi^2 k_B T/\hbar\omega_c)}{\sinh(2\pi^2 k_B T/\hbar\omega_c)}$, and $R_D = e^{-\pi/\omega_c\tau}$ are the spin, thermal, and Dingle damping terms, respectively, with g factor g^*, effective quasiparticle mass m^*, electron mass m_e, electron-phonon coupling strength λ_{e-ph}, temperature T, Boltzmann constant k_B, frequency F, field B, cyclotron frequency $\omega_c = eB/m^*$, and quasiparticle lifetime τ. δ_{LK} is a phase shift which is related to the curvature of the Fermi surface and can take values between ±1/8 for a corrugated 3D Fermi surface and is zero in the case of a 2D Fermi surface.[35] Here, $2\pi\beta$ is the Berry phase, which is zero in the case of trivial topology (such as in conventional metals with parabolic dispersion relations). In 2D Dirac systems with linear dispersions, such as graphene,[1] the Berry phase has a value of π. In 3D systems, the topological phase contribution is not necessarily quantized although it may be for certain field orientations.[35] Furthermore, it has been previously shown that a discrepancy exists between effective masses and quasiparticle lifetimes measured with de Haas–van Alphen and SdH oscillations, and the additional presence of a strong Zeeman splitting makes direct fitting with the L-K formula difficult.[20] Nonetheless, a Landau level fan diagram may still be used to extract the Berry phase, which we show for $H \parallel [001]$ for the 240 T and 211 T pockets in ZrSiS and ZrSiSe, respectively. We make use of the Lifshitz-Onsager quantization rule $A_F\frac{\hbar}{eB} = 2\pi(n+1/2+\delta_{LK})$, where n is the Landau level index, and the Onsager relation $F = A_F\frac{\hbar}{2\pi e}$, where A_F is the cross-sectional area of the Fermi surface normal to the field. Figures 4 and 5 summarize the extraction of the Berry phase using a Landau level diagram. We assign half-integer indices to the ρ_a peak positions and integer indices to the ρ_c peaks, as the quantum oscillations of ρ_a and ρ_c are 180° out of phase with each other, as we might expect.[36,37] In both compounds and for both applied current directions, the intercepts are nearly 1/2, which is consistent with the presence of a nontrivial Berry phase.

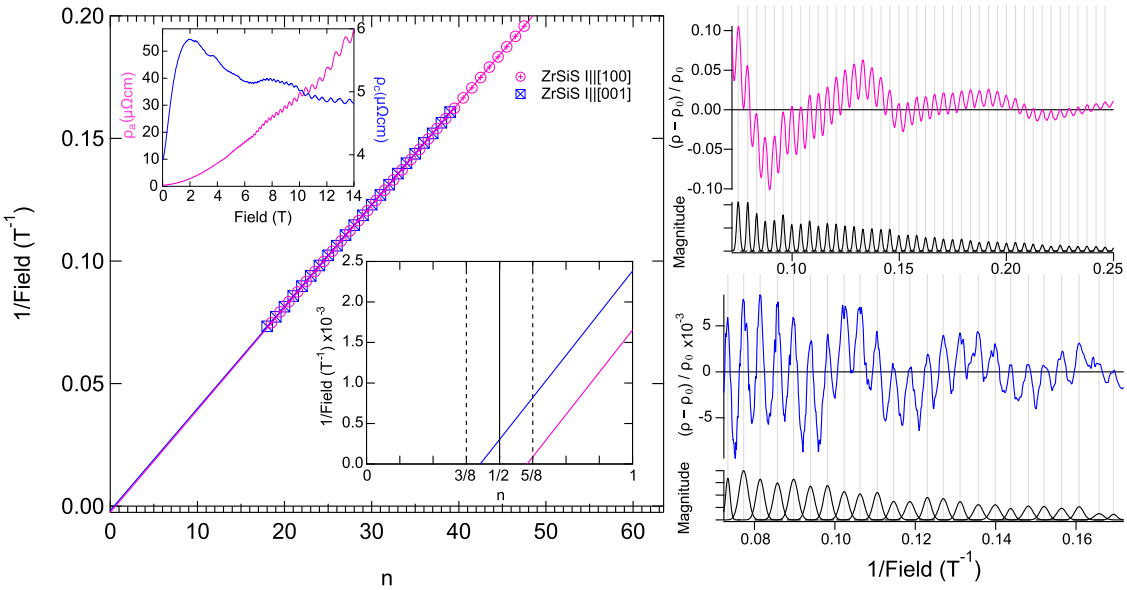

FIG. 4. Landau level fan diagram for ZrSiS for currents applied along [100] and [001] for magnetic field applied along [001]: Peak positions from the oscillatory resistivity ratios of Shubnikov–de Haas data are plotted against a Landau level index *n*. The intercept near 1/2 shows the existence of a nontrivial Berry phase associated with the β pocket of the Fermi surface and is evident from measurements along both crystalline axes. The right-hand side plots show the normalized, background-subtracted resistivity plotted against inverse magnetic field. The upper left inset shows ρ_a (pink) and ρ_c (blue). Note that they are plotted on different scales so that details of ρ_c are visible.

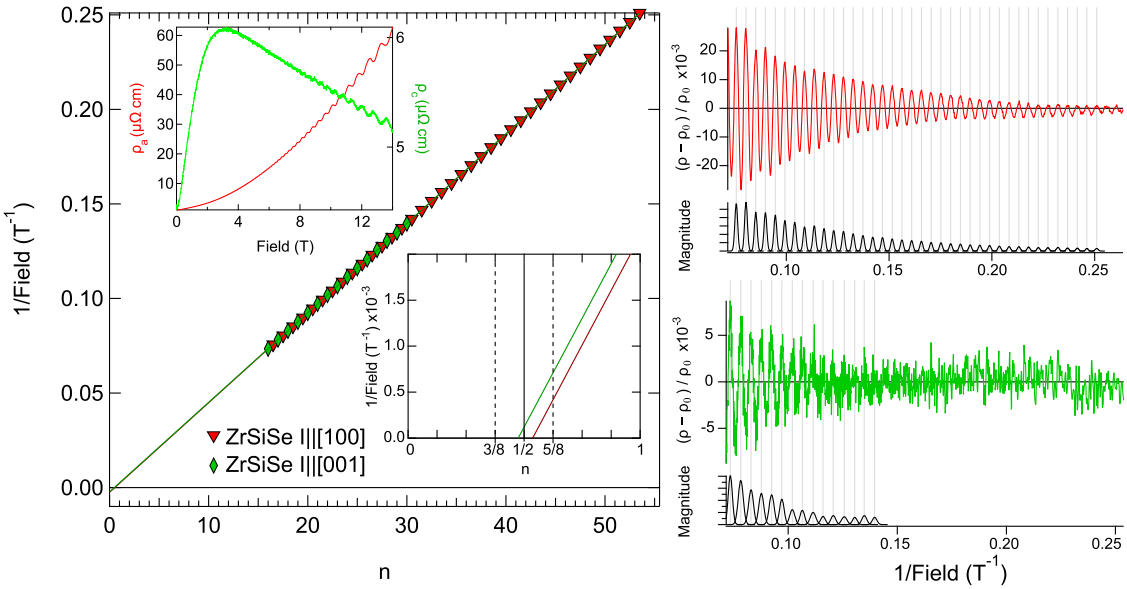

FIG. 5. Landau level fan diagram for ZrSiSe for currents applied along [100] and [001] for magnetic field applied along [001]: Peak positions from the oscillatory resistivity ratios of Shubnikov–de Haas data are plotted against a Landau level index *n*. The intercept near 1/2 shows the existence of a nontrivial Berry phase associated with the β pocket of the Fermi surface and is evident from measurements along both crystalline axes. The right-hand side plots show the normalized, background-subtracted resistivity plotted against inverse magnetic field. The upper left inset shows ρ_a (red) and ρ_c (green). Note that they are plotted on different scales so that the ρ_c details can be seen.

IV. DISCUSSION

The data reveal the importance of careful characterization of the angular-dependent magnetoresistance for different applied current directions. In ZrSiS, the in-plane resistivity anisotropy remains large (>60) in 14 T fields, while in ZrSiSe, the in-plane magnetoresistance is two fold symmetric and strongly suppressed when the applied field is parallel to the current. In ZrSiS, the 3D nature

of the band structure is likely responsible for its "butterfly shaped" magnetoresistance—also present in ZrSiSe, but absent in ZrSiTe—for $I \parallel [100]$ when the applied field is rotated from [100] to [001].[15,17] The suppression of in-plane resistivity anisotropy in ZrSiSe is consistent with the increasing two-dimensionality of the system as Se is substituted for S, which increases the c/a ratio and decreases the interlayer bonding strength.[9,15,21] However, this 2D behavior is not reflected in the resistivity anisotropy in the absence of field, where the resistivity anisotropy of ZrSiSe is, in fact, smaller than in ZrSiS. This demonstrates the complicated interplay between the both two- and three-dimensional nature of the Fermi surface and the resulting effect on the scattering probed by electronic transport.[15,25]

Another remarkable feature of the magnetoresistance is its strong decrease above 2 T for current and field applied parallel to each other along [001], shown in the upper left insets Figs. 4 and 5 and in the supplementary material. This decrease is reminiscent of predictions for the so-called chiral-anomaly in Dirac and Weyl semimetals. However, materials with Dirac line-nodes may have distinct transport properties from other topological materials and may not support a chiral anomaly.[11] Additionally, although ZrSiS and ZrSiSe both host a 3D nodal-line state and a nonsymmorphic symmetry-protected 2D Dirac node, the Fermi surface is composed of the nodal-line bands which are located at the Fermi level, while the Dirac node is located ~0.5 eV below the Fermi level and therefore thought not to contribute to the electronic transport.[10,18,20,22] The decreasing magnetoresistance also does not saturate up to 14 T and, in the case of ZrSiSe, follows a linear trend. Experiments in magnetic fields >25 T on the out-of-plane transport, similar to those of Pezzini *et al.*, may reveal further exotic transport properties and could provide insight into the suggested correlated nature of these materials.[22,26,27]

Our ability to simultaneously measure both in- and out-of-plane transport in our microstructured devices provides a useful tool to the experimental community and may open new avenues for functional devices which exploit the highly anisotropic nature of these materials for both applied currents and fields.[17] It has previously been stated,[20] and other transport measurements have shown,[16,17,22,23] that there is a very small quantum oscillation amplitude of the in-plane resistivity for in-plane applied fields, which can make SdH characterization prohibitive. With simultaneous measurements in two transport directions, we can easily resolve SdH oscillations in at least one transport direction, when the amplitude is reduced in the other (see the supplementary material). Furthermore, our well-defined transport geometries and high-aspect ratio devices provide a high signal-to-noise ratio, further improving our ability to resolve quantum oscillations. Our design and creation of free-standing devices allows the sample to be decoupled from the substrate, hence minimizing strain gradients due to differential thermal contraction.[38] Free standing devices also pave the way to other novel devices for use in ultralow temperature applications, thermodynamic measurement techniques, and hybrid devices exploiting superconducting or magnetic materials.

V. CONCLUSION

We have presented anisotropic measurements of magnetoresistance and quantum oscillation data in FIB-microstructured ZrSiS and ZrSiSe [100]- and [001]-oriented devices for applied magnetic fields up to 14 T. We have shown that there is a large resistivity anisotropy difference between the two materials and that the difference is linked to the angular dependence of the in-plane magnetoresistance. We observed that for currents along [001], the magnetoresistance decreases above 2 T, in contrast with large, nonsaturating magnetoresistances for other field orientations. We also showed the presence of a nontrivial Berry curvature for both compounds with currents along [100] and [001] in applied fields along [001] and an abrupt decrease in the magnetoresistance of ZrSiS and ZrSiSe above 2 T for currents applied along [001] with a parallel applied field. These measurements provide insight into the nature of these Dirac line-node semimetals and possible experimental directions for future experiments and applications.

SUPPLEMENTARY MATERIAL

The supplementary material contains figures which show further characterization of the ZrSiS and ZrSiSe microstructures including plots of resistivity vs temperature for fixed applied fields, angular dependent magnetoresistance, and Fast Fourier Transform data which show the quantum oscillation frequencies.

ACKNOWLEDGMENTS

K.R.S., M.K., P.J.W.M., and A.P.M were supported by the Max-Planck-Society. P.J.W.M. acknowledges support by the Swiss National Science Foundation (Grant Nos. PP00P2_176789). M.D.B. acknowledges studentship funding from EPSRC under Grant No. EP/I007002/1. Work at Princeton was supported by NSF through the Princeton Center for Complex Materials, a Materials Research Science and Engineering Center Grant No. DMR-1420541.

REFERENCES

[1] Y. Zhang, Y.-W. Tan, H. L. Stormer, and P. Kim, "Experimental observation of the quantum Hall effect and Berry's phase in graphene," Nature **438**, 201–204 (2005).
[2] C. L. Kane and E. J. Mele, "Z_2 topological order and the quantum spin Hall effect," Phys. Rev. Lett. **95**, 146802 (2005).
[3] M. König, S. Wiedmann, C. Brune, A. Roth, H. Buhmann, L. W. Molenkamp, X.-L. Qi, and S.-C. Zhang, "Quantum spin Hall insulator state in HgTe quantum wells," Science **318**, 766–770 (2007).
[4] S. M. Young, S. Zaheer, J. C. Y. Teo, C. L. Kane, E. J. Mele, and A. M. Rappe, "Dirac semimetal in three dimensions," Phys. Rev. Lett. **108**, 140405 (2012).
[5] Z. Wang, Y. Sun, X.-Q. Chen, C. Franchini, G. Xu, H. Weng, X. Dai, and Z. Fang, "Dirac semimetal and topological phase transitions in A_3Bi (A=Na, K, Rb)," Phys. Rev. B **85**, 195320 (2012).
[6] Z. K. Liu, B. Zhou, Y. Zhang, Z. J. Wang, H. M. Weng, D. Prabhakaran, S.-K. Mo, Z. X. Shen, Z. Fang, X. Dai, Z. Hussain, and Y. L. Chen, "Discovery of a three-dimensional topological Dirac semimetal, Na_3Bi," Science **343**, 864–867 (2014).
[7] L. He, X. Hong, J. Dong, J. Pan, Z. Zhang, J. Zhang, and S. Li, "Quantum transport evidence for the three-dimensional Dirac semimetal phase in Cd_3As_2," Phys. Rev. Lett. **113**, 246402 (2014).
[8] H. Wang, H. Wang, H. Liu, H. Lu, W. Yang, S. Jia, X.-J. Liu, X. C. Xie, J. Wei, and J. Wang, "Observation of superconductivity induced by a point contact on 3D Dirac semimetal Cd_3As_2 crystals," Nat. Mater. **15**, 38–42 (2015).
[9] Q. Xu, Z. Song, S. Nie, H. Weng, Z. Fang, and X. Dai, "Two-dimensional oxide topological insulator with iron-pnictide superconductor LiFeAs structure," Phys. Rev. B **92**, 205310 (2015).
[10] L. M. Schoop, M. N. Ali, C. Straßer, A. Topp, A. Varykhalov, D. Marchenko, V. Duppel, S. S. P. Parkin, B. V. Lotsch, and C. R. Ast, "Dirac cone protected

by non-symmorphic symmetry and three-dimensional Dirac line node in ZrSiS," Nat. Commun. **7**, 11696 (2016).
[11]T. Bzdušek, Q. Wu, A. Rüegg, M. Sigrist, and A. A. Soluyanov, "Nodal-chain metals," Nature **538**, 75–78 (2016).
[12]Y. Wu, L.-L. Wang, E. Mun, D. D. Johnson, D. Mou, L. Huang, Y. Lee, S. L. Bud'ko, P. C. Canfield, and A. Kaminski, "Dirac node arcs in $PtSn_4$," Nat. Phys. **12**, 667–671 (2016).
[13]G. Bian, T.-R. Chang, R. Sankar, S.-Y. Xu, H. Zheng, T. Neupert, C.-K. Chiu, S.-M. Huang, G. Chang, I. Belopolski, D. S. Sanchez, M. Neupane, N. Alidoust, C. Liu, B. Wang, C.-C. Lee, H.-T. Jeng, C. Zhang, Z. Yuan, S. Jia, A. Bansil, F. Chou, H. Lin, and M. Z. Hasan, "Topological nodal-line fermions in spin-orbit metal $PbTaSe_2$," Nat. Commun. **7**, 10556 (2016).
[14]M. Neupane, I. Belopolski, M. M. Hosen, D. S. Sanchez, R. Sankar, M. Szlawska, S.-Y. Xu, K. Dimitri, N. Dhakal, P. Maldonado, P. M. Oppeneer, D. Kaczorowski, F. Chou, M. Z. Hasan, and T. Durakiewicz, "Observation of topological nodal fermion semimetal phase in ZrSiS," Phys. Rev. B **93**, 201104(R) (2016).
[15]J. Hu, Z. Tang, J. Liu, X. Liu, Y. Zhu, D. Graf, K. Myhro, S. Tran, C. N. Lau, J. Wei, and Z. Mao, "Evidence of topological nodal-line fermions in ZrSiSe and ZrSiTe," Phys. Rev. Lett. **117**, 016602 (2016).
[16]X. Wang, X. Pan, M. Gao, J. Yu, J. Jiang, J. Zhang, H. Zuo, M. Zhang, Z. Wei, W. Niu, Z. Xia, X. Wan, Y. Chen, F. Song, Y. Xu, B. Wang, G. Wang, and R. Zhang, "Evidence of both surface and bulk Dirac bands and anisotropic nonsaturating magnetoresistance in ZrSiS," Adv. Electron. Mater. **2**, 1600228 (2016).
[17]M. N. Ali, L. M. Schoop, C. Garg, J. M. Lippmann, E. Lara, B. Lotsch, and S. S. P. Parkin, "Butterfly magnetoresistance, quasi-2D Dirac fermi surface and topological phase transition in ZrSiS," Sci. Adv. **2**, e1601742 (2016).
[18]Y.-Y. Lv, B.-B. Zhang, X. Li, S.-H. Yao, Y. B. Chen, J. Zhou, S.-T. Zhang, M.-H. Lu, and Y.-F. Chen, "Extremely large and significantly anisotropic magnetoresistance in ZrSiS single crystals," Appl. Phys. Lett. **108**, 244101 (2016).
[19]M. Matusiak, J. R. Cooper, and D. Kaczorowski, "Thermoelectric quantum oscillations in ZrSiS," Nat. Commun. **8**, 15219 (2017).
[20]J. Hu, Z. Tang, J. Liu, Y. Zhu, J. Wei, and Z. Mao, "Nearly massless Dirac fermions and strong Zeeman splitting in the nodal-line semimetal ZrSiS probed by de Haas–van Alphen quantum oscillations," Phys. Rev. B **96**, 045127 (2017).
[21]M. M. Hosen, K. Dimitri, I. Belopolski, P. Maldonado, R. Sankar, N. Dhakal, G. Dhakal, T. Cole, P. M. Oppeneer, D. Kaczorowski, F. Chou, M. Z. Hasan, T. Durakiewicz, and M. Neupane, "Tunability of the topological nodal-line semimetal phase in ZrSiX-type materials (X = S, Se, Te)," Phys. Rev. B **95**, 161101 (2017).
[22]S. Pezzini, M. R. van Delft, L. M. Schoop, B. V. Lotsch, A. Carrington, M. I. Katsnelson, N. E. Hussey, and S. Wiedmann, "Unconventional mass enhancement around the Dirac nodal loop in ZrSiS," Nat. Phys. **14**, 178–183 (2017).
[23]R. Singha, A. K. Pariari, B. Satpati, and P. Mandal, "Large nonsaturating magnetoresistance and signature of nondegenerate Dirac nodes in ZrSiS," Proc. Natl. Acad. Sci. U. S. A. **114**, 2468–2473 (2017).
[24]M. van Delft, S. Pezzini, T. Khouri, C. Müller, M. Breitkreiz, L. Schoop, A. Carrington, N. Hussey, and S. Wiedmann, "Electron-hole tunneling revealed by quantum oscillations in the nodal-line semimetal HfSiS," Phys. Rev. Lett. **121**, 256602 (2018).
[25]B.-B. Fu, C.-J. Yi, T.-T. Zhang, M. Caputo, J.-Z. Ma, X. Gao, B. Q. Lv, L.-Y. Kong, Y.-B. Huang, P. Richard, M. Shi, V. N. Strocov, C. Fang, H.-M. Weng, Y.-G. Shi, T. Qian, and H. Ding, "Dirac nodal surfaces and nodal lines in ZrSiS," Sci. Adv. **5**, eaau6459 (2019).
[26]M. M. Scherer, C. Honerkamp, A. N. Rudenko, E. A. Stepanov, A. I. Lichtenstein, and M. I. Katsnelson, "Excitonic instability and unconventional pairing in the nodal-line materials ZrSiS and ZrSiSe," Phys. Rev. B **98**, 241112(R) (2018).
[27]A. Rudenko, E. Stepanov, A. Lichtenstein, and M. Katsnelson, "Excitonic instability and pseudogap formation in nodal line semimetal ZrSiS," Phys. Rev. Lett. **120**, 216401 (2018).
[28]P. A. Volkov and S. Moroz, "Coulomb-induced instabilities of nodal surfaces," Phys. Rev. B **98**, 241107(R) (2018).
[29]A. Topp, J. M. Lippmann, A. Varykhalov, V. Duppel, B. V. Lotsch, C. R. Ast, and L. M. Schoop, "Non-symmorphic band degeneracy at the fermi level in ZrSiTe," New J. Phys. **18**, 125014 (2016).
[30]P. J. W. Moll, B. Zeng, L. Balicas, S. Galeski, F. F. Balakirev, E. D. Bauer, and F. Ronning, "Field-induced density wave in the heavy-fermion compound $CeRhIn_5$," Nat. Commun. **6**, 6663 (2015).
[31]F. Ronning, T. Helm, K. R. Shirer, M. D. Bachmann, L. Balicas, M. K. Chan, B. J. Ramshaw, R. D. McDonald, F. F. Balakirev, M. Jaime, E. D. Bauer, and P. J. W. Moll, "Electronic in-plane symmetry breaking at field-tuned quantum criticality in $CeRhIn_5$," Nature **548**, 313–317 (2017).
[32]K. R. Shirer, Y. Sun, M. D. Bachmann, C. Putzke, T. Helm, L. E. Winter, F. F. Balakirev, R. D. McDonald, J. G. Analytis, N. L. Nair, E. D. Bauer, F. Ronning, C. Felser, T. Meng, B. Yan, and P. J. W. Moll, "Dirac fermions in the heavy-fermion superconductors $Ce(Co,Rh,Ir)In_5$," e-print arXiv:1808.00403v1.
[33]P. J. W. Moll, P. Kushwaha, N. Nandi, B. Schmidt, and A. P. Mackenzie, "Evidence for hydrodynamic electron flow in $PdCoO_2$," Science **351**, 1061–1064 (2016).
[34]A. J. K. Haneveld and F. Jellinek, "Zirconium silicide and germanide chalcogenides preparation and crystal structures," Recl. Trav. Chim. Pays-Bas **83**, 776–783 (1964).
[35]A. Alexandradinata, C. Wang, W. Duan, and L. Glazman, "Revealing the topology of fermi-surface wave functions from magnetic quantum oscillations," Phys. Rev. X **8**, 011027 (2018).
[36]D. Shoenberg, *Magnetic Oscillations in Metals* (Cambridge University Press, 1984).
[37]F. E. Richards, "Investigation of the magnetoresistance quantum oscillations in magnesium," Phys. Rev. B **8**, 2552–2571 (1973).
[38]M. D. Bachmann, G. M. Ferguson, F. Theuss, T. Meng, C. Putzke, T. Helm, K. R. Shirer, Y.-S. Li, K. A. Modic, M. Nicklas, M. Koenig, D. Low, S. Ghosh, A. P. Mackenzie, F. Arnold, E. Hassinger, R. D. McDonald, L. E. Winter, E. D. Bauer, F. Ronning, B. J. Ramshaw, K. C. Nowack, and P. J. W. Moll, "Spatially modulated heavy-fermion superconductivity in $CeIrIn_5$," Science **366**, 6462 (2019).